Progress in Organic Coatings 207 (2025) 109397

Contents lists available at ScienceDirect

Progress in Organic Coatings

journal homepage: www.elsevier.com/locate/porgcoat

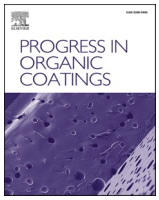

Synergy of consecutive PEO and LDH surface treatments on the corrosion protection and adhesion strength of organic coatings on AA2024T3☆

Muhammad Ahsan Iqbal [a], Humaira Asghar [b], Endzhe Matykina [a], Raúl Arrabal [a], Marta Mohedano [a], Jesús Manuel Vega [a,*]

[a] Departamento de Ingeniería Química y de Materiales, Facultad de Ciencias Químicas, Universidad Complutense de Madrid, 28040 Madrid, Spain
[b] Department of Chemistry, University of Torino, Via Giuria 7, 10125 Torino, Italy

ARTICLE INFO

Keywords:
EIS
Adhesion
Plasma electrolytic oxidation (PEO)
Layered Double Hydroxide (LDH)
Aluminium alloys

ABSTRACT

The properties of the interface AA2024-T3/organic coating is improved with a tailored combination of different surface treatments: i) a dual anodizing process comprising an energy-efficient (41 % reduction in energy consumption) plasma electrolytic oxidation (PEO) process just after conventional anodizing (to build a precursor layer), followed by ii) a conversion coating (CC) based on the in-situ growth of a MgAl-layered double hydroxide (LDH). This combination allows the formation of a thick PEO coating (40 μm) with an outermost LDH-CC layer. Prior to applying the organic coating, a characterization of the roughness, crystalline structure, morphology and composition of the protective systems (PEO and PEO-LDH) is thoroughly investigated. Corrosion performance is evaluated using electrochemical impedance spectroscopy (EIS) for all the systems, uncoated and epoxy-coated ones. In addition, the wet and dry adhesion properties of the epoxy-coated systems are evaluated. Results reveal that the PEO-LDH + Epoxy system shows superior wet adhesion and better corrosion resistance after 28 days of immersion in 3.5 wt% NaCl. Furthermore, the EIS diagrams for the PEO-LDH system demonstrate a synergistic effect of the PEO and LDH treatments, as evidenced by the capacitance and resistance values associated with the low-frequency time constant, outperforming the stand-alone PEO system.

1. Introduction

Many efforts have gone into developing a viable approach for increasing the corrosion resistance of aluminium and its alloys in corrosive conditions. Protecting a reactive metal with organic coatings is a straightforward approach to achieving corrosion prevention purposes [1–6]. However, regardless of how the organic coatings was deployed, electrolytes (e.g., water having dissolved oxygen) can easily penetrate the organic coating through pores, cracks, and other defects, enabling conductive pathways of aggressive species (e.g., chlorides) toward the metal/coating interface, triggering early stage of corrosion and the rapid loss of the system's adhesion [7,8]. Anodizing, conversion coatings (CC), sol-gel coating, and other surface pre-treatments/coatings are efficient in terms of enhancing the adhesion and protective capabilities of organic coatings on the surface of aluminium alloys [9–12]. However, novel strategies are needed to further improve the adhesion of the organic coatings as well as to introduce unique characteristics to the coating systems.

Plasma electrolytic oxidation (PEO) is an efficient eco-friendly coating process to develop ceramic-like hard coatings with long-term protective capabilities on light metallic alloys [13–18]. However, the PEO process has a relatively high energy consumption and is 20–50 times more energy-intensive than conventional anodizing, which restricts its applications in high-end technologies. Numerous approaches, such as the design of cell geometry and processing parameters, electrolyte composition, and pre-anodizing treatments, were reported for the low-energy production of PEO coatings [19–23]. However, the effectiveness of the coatings should not be compromised and the coating's ability to resist corrosion must remain effectual [24]. Particularly encouraging results for overcoming the energy consumption of the PEO process were obtained in the case of pre-anodized aluminium alloys, where pre-anodization was found to support the early establishment of a “soft sparking” regime which results in faster coating growth rates and low energy consumption [25].

☆ This article is part of a Special issue entitled: ‘AETOC2024’ published in Progress in Organic Coatings.

* Corresponding author.
E-mail address: jevega@ucm.es (J.M. Vega).

https://doi.org/10.1016/j.porgcoat.2025.109397
Received 1 December 2024; Received in revised form 22 May 2025; Accepted 23 May 2025
Available online 29 May 2025

The oxide layers developed by PEO are usually hard, strongly adherent to the substrate, and confer both corrosion and wear resistance. Further, the application of top organic coatings on the PEO layer can limit the penetration paths of the corrosive elements to the metal surface by sealing the PEO coating pores and creating a hybrid coating system with improved aesthetic and protective properties [26,27]. Even if such organic coating systems have appropriate barrier properties, their long-term durability is still in question since organic coatings exhibit poor wet adhesion strength and deteriorate rapidly over time. Furthermore, the coating's capacity to provide active protection is more significant than providing only barrier protection. The idea of a smart coating, which is a wide topic of interest, is an effective approach for the active corrosion protection system, where corrosive species trigger the release of incorporated inhibitive ions through various mechanisms and is an effective strategy for the active corrosion protection system.

In that aspect, the use of layered double hydroxides (LDHs) was proven to be an effective and smart way to prevent metal corrosion due to LDH's unique lamellar structure, anionic exchange capability, self-healing characteristics, eco-friendly in nature and adhesion characteristics [28–31]. The properties of the PEO layer significantly affect the surface morphology of LDHs. Studies using thin PEO layers (below 10 μm) have shown that the formation of thin, non-uniform LDH flakes on PEO is influenced by key factors such as surface porosity, the composition of the PEO layer, and the geometry of the porous structure, all of which play a critical role in determining the final morphology of the LDHs [32–34]. The outer porous PEO surface results in the formation of nanoflake LDHs that partially seal the porous structure, preventing the development of a distinct, uniform film. Indeed, several research studies [26,32–35] have suggested this sealing post-treatment for PEO-based Al alloys but do not investigate the interaction of organic coatings with LDHs-modified PEO system. The strong adhesion of in-situ grown LDH film with the underlying substrates and the ability to control/entrap the corrosive species can provide long-term corrosion protection through self-healing characteristics [35–38]. Serdechnova et al. [37] investigated the in-situ growth of LDHs on thin PEO layers, enhancing their barrier properties, providing active protection, and partially sealing PEO defects. Similarly, Chen et al. [39] developed inhibitor-loaded LDH nanoplatelets on PEO-coated AA2024, which preferentially formed in micro-pores and cracks, further enhancing protection. However, the intrinsic porosity and tortuosity of thick PEO layers hindered subsequent treatment processes. Mohedano et al. [35] found that thicker PEO layers, formed at higher voltages, reduced LDH formation due to limited $Al(OH)^{2+}$ availability. Furthermore, Serdechnova et al. [40] observed that crystalline oxides, such as γ-Al_2O_3 and α-Al_2O_3, in PEO coatings on AA2024 hindered LDH growth, while amorphous oxide layers were more conducive to LDH formation. Bouali et al. [36] utilized sol-gel post-processing to develop an aluminium oxide-based xerogel layer, providing a better source of $Al(OH)_4^-$ for LDH development. These studies highlight that the type, phase composition, and thickness of PEO coatings are critical for successful in-situ LDH synthesis, as they significantly influence the availability of aluminium sources for LDH formation. In particular, in-situ LDH formation is most effective in coatings under 20 μm in thickness. While thicker PEO coatings are commonly used for enhanced protection in harsh environments, understanding the formation of LDHs on thick PEO and their impact on structural and corrosion resistance properties is essential.

Moreover, the role of LDHs in post-modification for organic systems, particularly in enhancing adhesion characteristics, remains an important area for further investigation. This is crucial for ensuring the long-term durability and applicability of coatings on exposure with corrosive media. A recent study based on a three layers system (Zn—Al LDH conversion layer, followed by a hybrid sol-gel silane film with an epoxy topcoat) has demonstrated the efficacy of LDHs as a pretreatment for active corrosion protection. This approach resulted in significantly improved active corrosion resistance and enhanced adhesion properties, highlighting the potential role of LDHs for advanced multifunctional coating systems [41]. Regarding to organic coatings and PEO, a bilayer coating system by Zeng et al. [42] demonstrated that a silane layer effectively sealed a thin PEO-formed alumina coating on UNS A97075 Al alloy, significantly delaying corrosion and improving resistance over 576 h of immersion. Pezzato et al. [43] explored the combination of PEO coatings with sol-gel layers on 7020 AA and AZ80 alloys. The findings demonstrated that the PEO layer is able to improve the uniformity and durability of the organic coatings, providing superior barrier resistance under harsh conditions; however, a detailed investigation of dry/wet adhesion characteristics was not evaluated.

In conclusion, the in-situ growth of LDHs on thick PEO layers (characterized by a loose outer porous layer) presents a significant advancement in enhancing the overall system durability and can offers a suitable platform for further modification with organic coating systems. This underscores two critical aspects to investigate: (1) the in-situ growth LDHs on thick PEO layers (with high energy reduction), focusing on their structural integrity and corrosion resistance properties, and (2) a comprehensive investigation of role of LDHs on adhesion characteristics upon applying the organic top layer and understanding of associated corrosion resistance mechanism in multilayer systems. Furthermore, the formation of LDHs is established to provide a smart way to incorporate the choice of corrosion inhibitors, effectively addressing the challenges of directly incorporating them into organic coatings, thus improving long-term performance and protection. In fact, an understanding of the role of the LDH layer in multilayer systems is strongly needed to evaluate their applicability for high-performance applications.

Furthermore, to the best of the author's knowledge, the available literature based on LDH/PEO systems is mainly focused on developing thin PEO coatings [32–34]. This PEO thin layer provides an efficient source of aluminium for the formation of LDHs directly on the surface. On the other hand, the use of pre-anodic precursors to developing energy-efficient PEO leads to thick coatings >40 μm that make it difficult to get the requisite sources of aluminium for LDH modification [44–46]. However, the resulting outer porous layer can provide possible pathways for electrolyte to interact with inner barrier layers.

The goal of the present work is to explore the synergy of an energy-efficient thick PEO layer and an in-situ growth conversion coating (based on LDH without corrosion inhibitors) when organic coatings are used as topmost layer. The work represents a significant advancement in the field of protective coatings by achieving the formation of thick PEO coatings with minimal energy consumption, followed by the formation of LDHs directly on thick PEO is proposed. A characterization of the roughness, crystalline structure, morphology, composition of the protective systems was performed. The developed two different systems were further studied with and without an epoxy coating: PEO (epoxy) and PEO-LDH (Epoxy). The corrosion resistance was evaluated by electrochemical impedance spectroscopy (EIS) after 28 days of immersion in 3.5 wt% NaCl as well as the adhesion properties (dry and wet) of the overall systems after immersion in the electrolyte.

2. Methods

2.1. Specimen preparation

A 2.0 mm thick sheet of commercial 2024-T3 (wt%: 3.8–4.9 Cu, 1.2–1.8 Mg, 0.3–0.9 Mn, 0.5 Fe, 0.5 Si, 0.25 Zn, 0.15 Ti, 0.10 Cr, and Al balance) was cut into specimens measuring 40 mm × 25 mm × 2 mm. Using a commercial resin (Lacquer 45, MacDermid plc.), the working area was restricted to 7.8 cm^2 and a hole of about 3 mm was drilled through the sample on the top side to allow for electrical connection. The rectangular specimens were etched in solutions of 70 g L^{-1} BONDERITE C-AK 4215NC for 10 min at 60 °C and 85 g L^{-1} BONDERITE C-AK ALUM ETCH 2 AERO for 2 min at 40 °C. Each operation was followed by vigorous agitation and washing with deionized water. After being cleaned in deionized water, dried with warm air, and immersed in

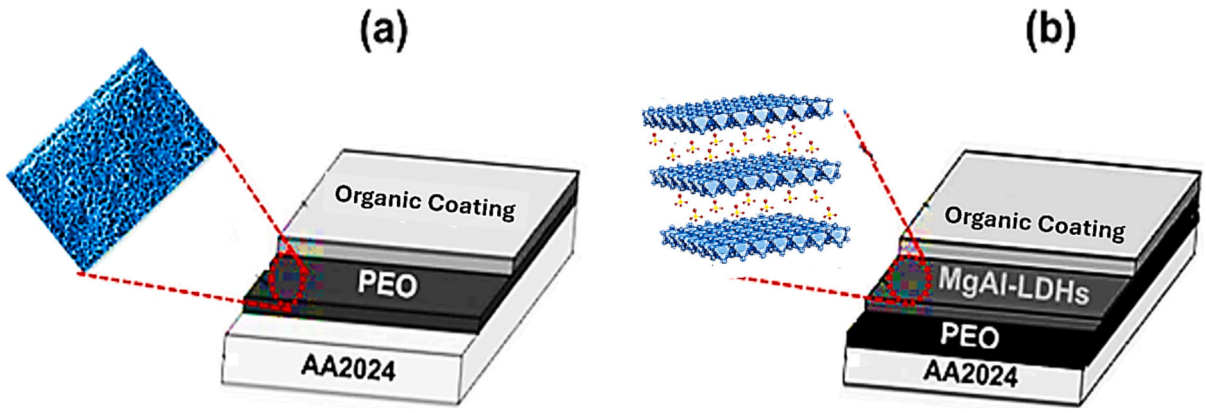

Fig. 1. Schematic diagram of the developed coatings: (a) PEO + Epoxy, (b) PEO-LDH + Epoxy.

BONDERITE C-IC SMUTGO NC AERO for five minutes.

2.1.1. Preparation of PEO coatings

Prior to the PEO process, the following pretreatment was carried out: anodizing AA2024 in 24.5 wt% sulfuric acid solution at 20 °C, 50 mA cm^{-2} for 800 s. This precursor layer (around 20 ± 3 μm) was able to reduce the energy consumption of the plasma process by 41 % [46].

The PEO treatment was performed using an ET Systems electronic 2 kW EAC-S2000 power supply, operating with a square electrical signal (490 V/-110 V, 50 % duty cycle, 500 mA cm^{-2}, 400 Hz) and an initial ramp-up of 60 s. The constantly agitated electrolyte consisted of 10.5 g L^{-1} sodium silicate (1.39 kg dm^{-3}), 5 g L^{-1} sodium phosphate dodecahydrate, and 2.8 g L^{-1} potassium hydroxide. A 2 L double-walled glass cell with a stainless steel counter electrode were used for the process. The treatment was sustained for at least 600 s after a noticeable current drop, marking the uniform onset of the "soft-sparking" regime, and resulted in a coating designated as "PEO".

2.1.2. Preparation of MgAl-LDH-films

The MgAl-LDHs were synthesized using an in-situ growth method. The PEO coating was first cleaned with acetone, followed by etching in a 0.1 M aqueous NaOH solution for 10 s. A mixed solution was prepared containing 0.1 M $Mg(NO_3)_2{\cdot}6H_2O$, 0.05 M $Al(NO_3)_3.9H_2O$, and 0.3 M NH_4NO_3, which was then transferred to a Teflon-lined stainless steel autoclave containing the PEO samples. The pH of the solution was adjusted to 10.0 before the autoclave was closed and heated for 12 h at 100 °C. Finally, the LDH-treated PEO samples were washed with deionized water and dried at ambient temperature. The sample is labelled as PEO-LDH.

2.1.3. Preparation of multilayer coating

A commercial epoxy resin (Epoxy 37,076) was mixed with a curing agent (Hardener 92,133) and thinner (C25/90S) in a mass ratio of 1:0.31: 0.30, and the mixture was thoroughly mixed. The epoxy coatings (EP) were applied to the PEO and PEO-LDH specimens using draw-down bar. PEO + Epoxy and PEO-LDH + Epoxy terminologies are further used for the resultant epoxy base coatings. Curing was carried out in an oven at 80 °C for 60 min. The general layout of developed epoxy-based coating systems is shown in Fig. 1. For comparison, a pure epoxy coating was also applied directly to aluminium surfaces under the same conditions.

2.2. Specimen characterization

X-ray diffraction (XRD) patterns were collected with a Philips X'Pert diffractometer (Cu Kα 1.54 Å), using a scan range 2θ from 10 to 80° at a scanning speed of 0.04° per second with an incidence angle of 0.5° and 2 s/step of counting time.

3D topographic images of the surface were obtained, prior to applying the epoxy coating, using an optical profilometer (InfiniteFocusSL, Bruker, Alicona) with a × 50 lens. The S_a roughness parameters was extracted using the IF-Measure Suite software, which provides information on the height difference of each point relative to the arithmetic mean of the surface.

The surface morphology and elemental composition of the coatings were studied through scanning electron microscopy (JEOL JSM-6400) equipped with an Oxford Link energy dispersive X-ray (EDS) system. Cross-sectional specimens were prepared by gradual grinding (from P120 to P4000), followed by polishing with 0.1 μm diamond paste once they were embedded in epoxy resin. Graphite was used for sputtering and therefore, the carbon composition (atomic %) was not taken into account in the EDS analysis.

The coating thickness was determined by the eddy current method (Isoscope FMP10, Fischer) as well as by SEM cross-sectional analysis. A PEO layer around 43 ± 6 μm is obtained and the thickness of the epoxy coating is 40 ± 10 μm.

Electrochemical Impedance Spectroscopy (EIS) measurements were conducted at 1, 3, 7, 14 and 28 days of immersion in 3.5 wt% NaCl aqueous solution using a standard three-electrode cell geometry connected to a GillAC computer-controlled potentiostat (ACM Instruments). The working area of the specimens was defined as 1 cm^2; the counter and reference electrodes were graphite and silver/silver chloride (Ag/AgCl in 3 M KCl), respectively. A sinusoidal perturbation of 10 mV amplitude in the frequency range of 100 kHz–0.01 Hz was applied, measuring 6 points per decade.

The adhesion of epoxy coatings on PEO + Epoxy and PEO-LDH + Epoxy coated samples was investigated by pull-off tests in dry and wet conditions (ASTM D3359–97). In order to determine the wet adhesion strength, the coating samples were exposed to 3.5 wt% NaCl solution for 28 days and the adhesion measurement was performed one week later. Adhesion tests were carried out through the cutting tool to make a cross-cut pattern through the composite coatings at ca. 90° angles.

3. Results and discussion

In our earlier work [46], it was described the role of anodic film thickness on the PEO film's current (voltage)-time responses with and without anodic precursors on AA2024 alloy. The use of these precursors (i.e., an anodized AA2024 surface) serves as a sort of sacrificial layer for the PEO process, where it is transformed to PEO coating (i.e., the anodizing film no longer exists as a separate layer). It is a deliberate strategy aimed at enabling: i) more energy-efficient PEO process (quick process, <800 s), and ii) robust PEO process. The predicted current decrease allowed the coating development to proceed with a lower current output. The time to current drop was reduced by 63.3 %, attributed to the early formation of the "soft sparking" regime, which

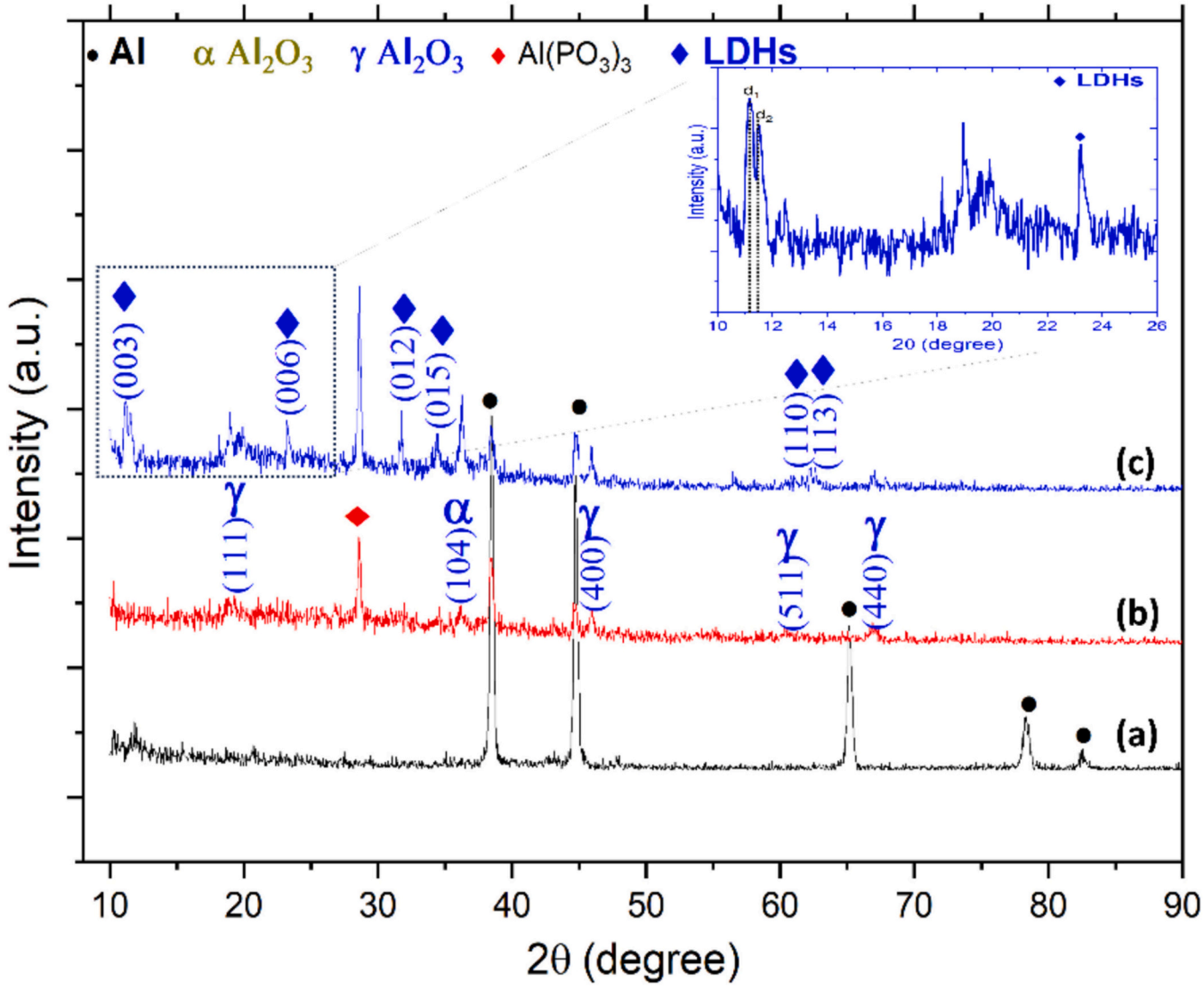

Fig. 2. X-ray diffraction patterns, (a) AA2024, (b) PEO, (c) PEO-LDH.

can be explained by the faster transition to this regime, enhancing the overall coating growth rate.

3.1. As received characterization

Fig. 2 depicts the grazing incidence X-ray diffraction patterns of the developed PEO and LDH-modified coatings. The PEO films primarily consist of γ-Al_2O_3, with the presence of the α-Al_2O_3 phase (Fig. 2(b)).

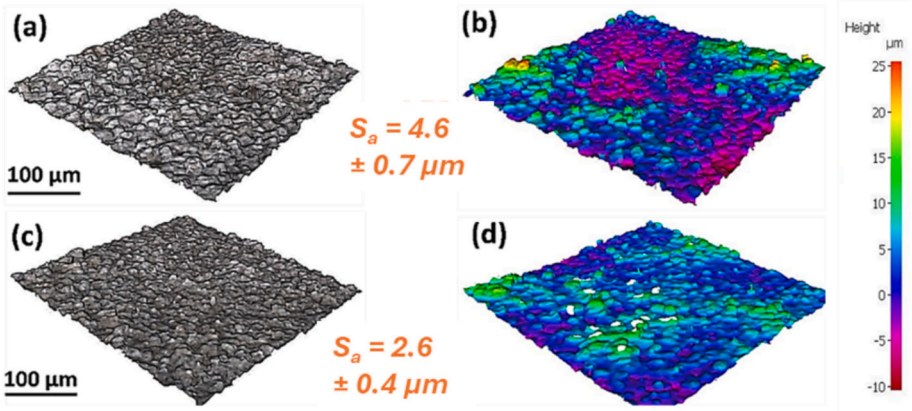

Fig. 3. Optical profilometry micrographs and surface roughness parameters of the PEO coated samples, (a, b) PEO and (c, d) PEO-LDH.

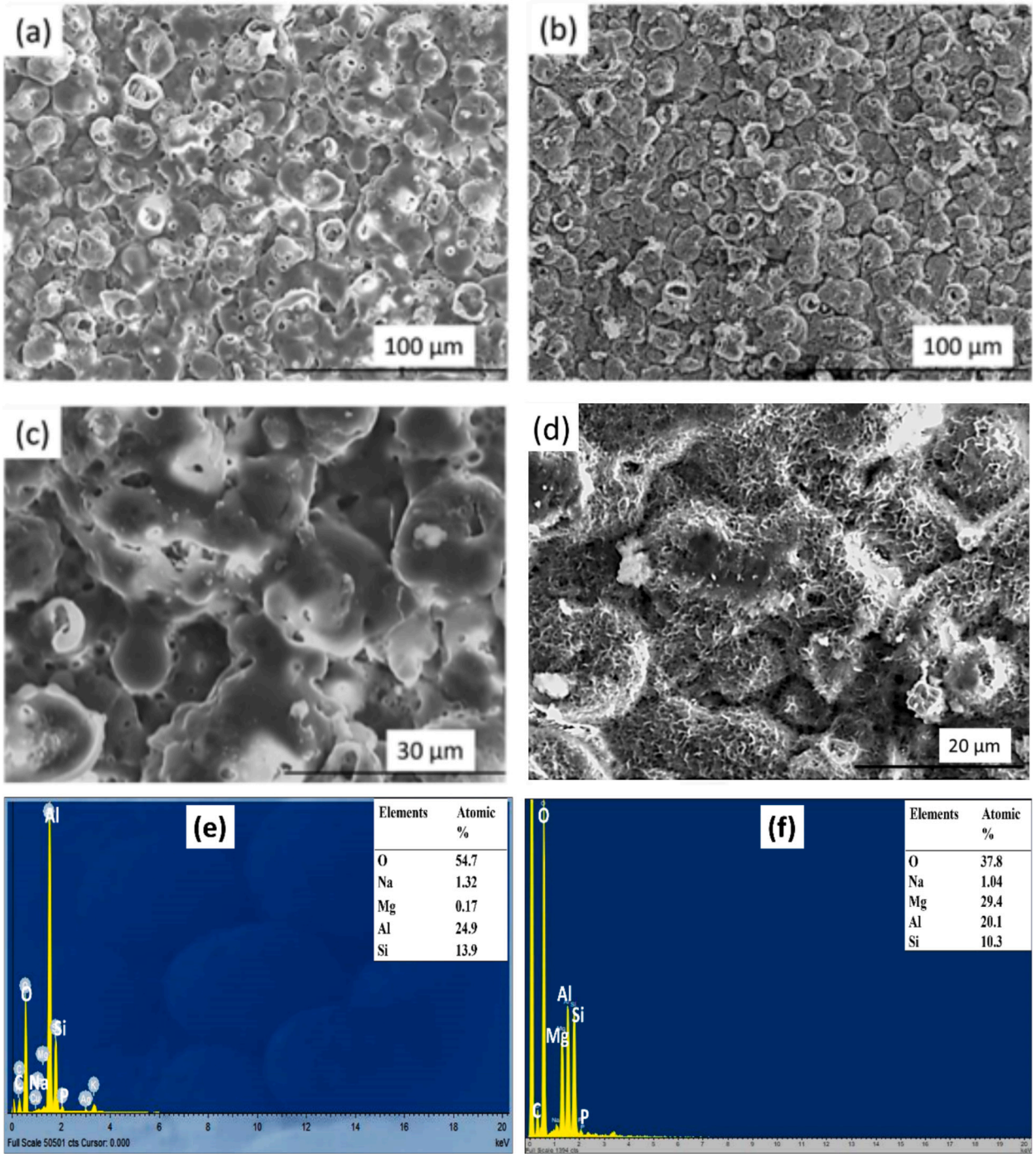

Fig. 4. Surface top view of (a, c) PEO (b, d) PEO-LDH, and EDS analysis of (e) PEO, and (f) PEO-LDH.

The recorded diffraction pattern matches with the combined JCPDS patterns of γ-Al_2O_3 (ICDD card 00–050-0741) and α-Al_2O_3 (ICDD card 00–046-1212) and is in concordance with other studies where PEO treatments on anodic surface [46,47]. Additionally, elements P and Si also took part in the plasma process from the electrolytes, forming the Al $(PO_3)_3$ (ICDD card 80–1526), and mullite phases($(3Al_2O_3{\cdot}2SiO_2)$(ICDD card 01–079-1454)), respectively.

According to the XRD pattern (Fig. 2 (c)), PEO-LDH shows peaks around 11°, 23.0°, 34.6°, and two high-angle reflections at 61.6° and 62.8°, which were assigned to (003), (006), (012) and (110), (113) planes, respectively. These peaks indicate the formation of a conventional LDH structure. The XRD data reveal two distinct LDH phases characterized by varying interlayer distances (basal spacing, d_1 = 0.79 nm (11.3°) and d_2 = 0.76 nm (11.6°) (Figure (c)). The initial phase, designated as the d_1-LDH phase, is considered to be a MgAl LDH intercalated with nitrates with the possibility of symmetry of the nitrate anion in a tilted position (relative to the layer plane), resulting in a reduction of basal spacing compared to traditional NO_3^- anions [48]. The phase exhibiting the maximum basal spacing value, specifically d_2-LDH, aligns effectively with the intercalation of carbonate anions. The d_2 peaks match MgAl-CO_3-LDH (JCPDS No: 00–014-0191), implying that the d_2-LDH phase is similar to $Mg_6Al_2CO_3(OH)_{16}.H_2O$) (c = 2.67 nm and a = 0.35 nm) [49]. This finding is not surprising, as the solution in which the LDH was grown had an initial pH of 10, and without nitrogen purging, a significant amount of CO_2 could dissolve in the LDH growth solution, leading to the formation of a CO_3^{2-}-based LDH system. This

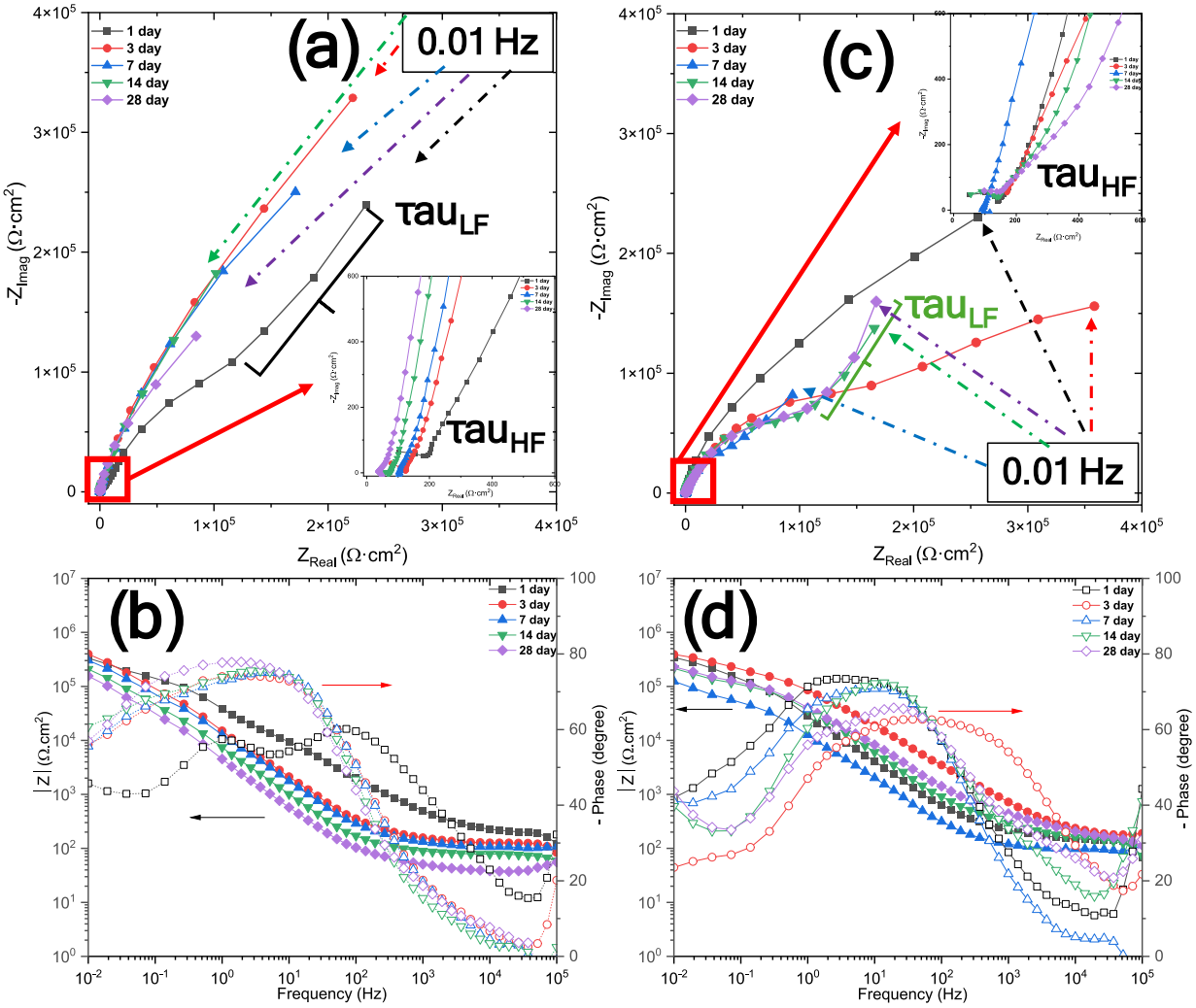

Fig. 5. Impedance diagrams (Nyquist and Bode) at different immersion time in 3.5 wt% NaCl: (a-b) PEO, and (c-d) PEO-LDH.

implies that during the synthesis, a mixture including the intercalation of carbonates and nitrates most likely happened.

Fig. 3 shows the micrographs of the surface morphology as well as the 3D (colour) images used to obtain the roughness. The roughness is influenced by features such as pore size and density, pore type (deep or shallow), micro-cracks, pinholes, and pancake projections of the PEO layer. The S_a value for the PEO-LDH system is approximately half of that for PEO (2.6 μm vs. 4.5 μm), indicating the partial sealing of PEO pores/defects, which results in a somewhat lower surface roughness for PEO-LDH specimen.

Fig. 4 (a, c) shows the longitudinal micrographs of bare PEO by SEM, revealing a typical sponge-like morphology with porous distributions located in the discharge channels. This morphology is linked to thermal stresses and gas evolution through the molten oxide material [50,51]. In contrast, Fig. 4 (b, d) depicts completely different surface morphologies due to LDH surface treatment, where a typical thin lamellar layered structure is observed, with nano-platelets covering the PEO surface [52].

Fig. 4 (e, f) shows the EDS spectra of the surface of PEO and PEO + LDH systems, respectively. The highest concentrations of Al and O are observed for the PEO sample, indicating the predominant formation of Al_2O_3, while Na and Si are present in similar concentrations for both samples. The most relevant result is the presence of an additional Mg peak on the surface of PEO-LDH, which aligns with the formation of LDHs observed in the XRD diffractograms (Fig. 2). Although it is obvious that silicon did not contribute to the in situ development of LDHs, its presence on the PEO-LDH specimens explains the blanket effect of LDH's nest-like structure, where the nanoplatelets successfully cover the PEO surface [53].

3.2. Corrosion evaluation

The corrosion performance of these two systems were evaluated by EIS after immersion in 3.5 wt% NaCl up to 28 days. Fig. 5 shows the variation of the Nyquist (Fig. 5 (a)) and Bode diagrams (Fig. 5 (b)) for the PEO system with time. Initially (i.e., 1 day measurement), the PEO system is showing 3 time constants (τ), one at high frequency (HF), other at medium frequency (called MF, between high and low ones) and a third one at low frequency (LF). In order to estimate if the latter time constant (τ_{LF}) can be attributed to a semi-infinite diffusion process (typically identify by an impedance tail with an angle of 45° in the Nyquist plot), the real and imaginary part of the impedance can be plotted vs. the inverse of the angular frequency (ω) root square: $\omega^{-1/2}$ [54]. Although there is a limitation due to the small number of points at LF (around 3–4), the real and imaginary parts of the impedance seem to provide a linear behaviour in Fig. 6 (a) (following Fick's law), with linear correlation coefficients (R) of 0.99983 and 0.99966 for the real part and imaginary part of the impedance, respectively. Therefore, although such a time constant may be linked to a mass transport process inside the pores, further analysis is needed to confirm this assumption. In contrast, after 3 days of immersion, the time constant at low frequency (τ_{LF}) cannot be observed in the impedance diagrams (either Fig. 5 (a) or Fig. 5 (b)) and the diameter of the semicircle of the time constant at medium

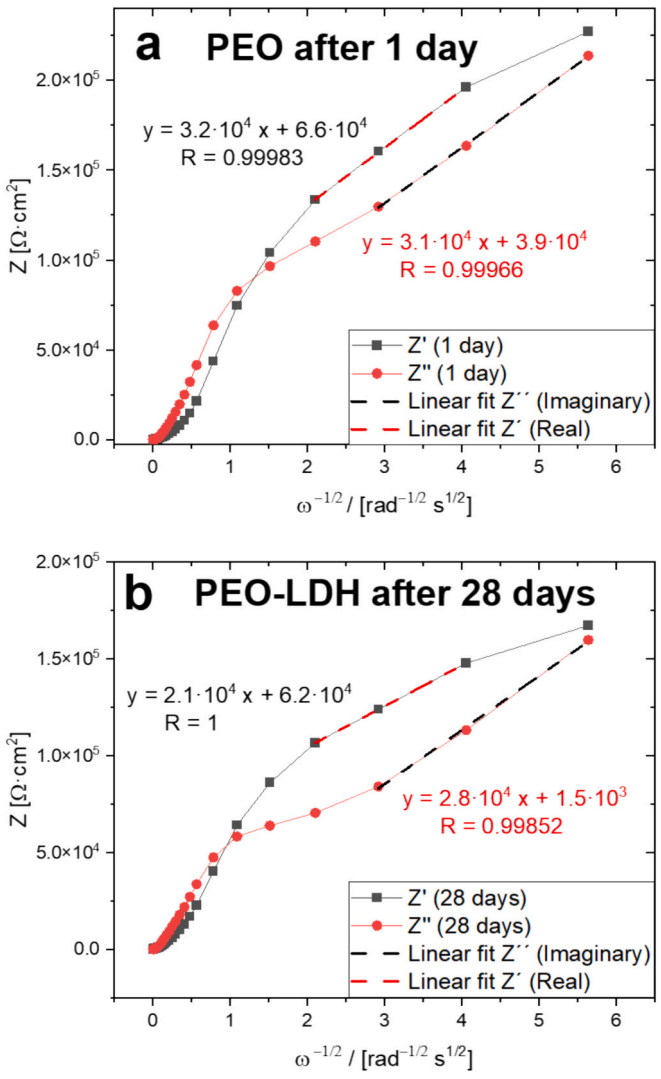

Fig. 6. Representation of the impedance (Z´ and Z") versus the $\omega^{-1/2}$ for: (a) PEO after 1 day of immersion, and (b) PEO-LDH after 28 days of immersion in 3.5 wt% NaCl.

frequency (τ_{MF}) increases. Beyond 3 days, the shape of the impedance diagrams (Nyquist and Bode) do not change at all except a slightly progressive decrease of impedance from the τ_{MF}, reaching the lowest value after 28 days (i.e., smallest semicircle in Fig. 5 (a) and the lowest impedance modulus at 0.01 Hz ($|Z_{0.01Hz}|$) in Fig. 5 (b)).

If these results are compared with the ones of PEO-LDH systems, certain similarities as well as significant differences can be found (Fig. 5 (c-d)). The EIS diagram after 1 day of immersion only reveals the presence of two-time constants (τ_{HF} and τ_{MF}), indicating that the diffusion phenomenon (previously observed in the PEO system) is hindered. Interestingly, although the total impedance remains stable after 3 days of immersion (it underwent a slightly increase according to $|Z_{0.01Hz}|$ values in Fig. 5 (d)), a new time constant becomes visible at LF and according to the phase angle-Bode plot, the frequency window of the angle at around −60° becomes broader than before. These characteristics suggest that the LDH layer on the PEO surface forms a dynamic system that evolves during immersion. In fact, after 7 days the shape of the impedance diagrams has changed again, and at this time, there is a drastic decrease of the impedance, reaching the lowest $|Z_{0.01Hz}|$ value (Fig. 5 (d)). Moreover, the time constant at LF has almost disappeared. Finally, at larger immersion time (i.e.,14 and 28 days), the three time constants are consolidated and the shape of the EIS diagrams resembles that one of PEO at 1 day of immersion, especially the Nyquist plots (Fig. 5 (a) vs. Fig. 5 (c)). It might indicate that between 14/28 days, the impact of the LDH layer can be hindered, where a diffusion phenomenon seems to occur, according to the findings of Fig. 6 (b), where a linear behaviour is observed with excellent correlation coefficients.

However, when an organic coating is applied (Fig. 7), the impedance diagrams become more consistent, showing an impedance diagram characterized by two distinct time constants. In general, a depressed semicircle is observed at any time, revealing the overlap of several time constants (at least two, τ_{HF} and τ_{MF}). Therefore, the main difference between PEO + Epoxy and PEO-LDH + Epoxy is the abrupt drop of the $|Z_{0.01Hz}|$ after 7 days of the former ((Fig. 7 (a) and (b))) whilst the latter not only undergoes a slightly decrease of the $|Z_{0.01Hz}|$ with time but also it remains stable between 14 and 28 days (Fig. 7 (c) and (d)). The barrier protection of the coatings is affected with the immersion time and usually, the impedance decreases with time as a sign of degradation. So, the variation of the impedance diagrams is affected by the water uptake (the resistance of the epoxy coating decreases and the capacitance increases). Once the electrolyte has reached the PEO/Epoxy interface, the degradation will take place at such interface and in the PEO layer itself, having a different impact in presence or absence of the LDH layer.

In order to provide additional information to those subtle differences as well as the nature of the overlapped time constants, several equivalent circuits (EC) with physical meaning were used (Fig. 8), assuming a nonideal capacitive behaviour: the impedance can be defined as $Z_{CPE} = Y_0^{-1}(j\omega)^{-\alpha}$, where Y_0 is the frequency independent constant, $j^2 = (-1)$, $\omega = 2\pi f$ is the angular frequency in rad/s, f is the frequency in Hz, and the dimensionless α ($0 < \alpha < 1$) is related to the width of distribution of relaxation time [55]. Moreover, the time constant at LF for PEO and PEO-LDH systems was not considered for fitting due to the low number of points and therefore, that part of the impedance diagram was discarded for this analysis. Finally, in order to avoid any sensitivity to artifacts, the fitting was done at frequencies below 10 kHz [56] (Fig. S1 shows the impedance plots and the fitting range where is possible to distinguish the distribution of time constants as well as the possible presence of artifacts).

The electrochemical parameters in the EC without an organic coating are the following (Fig. 8 (a)): R_s as the electrolyte solution resistance; CPE_{out} and CPE_{in} represent the constant phase element (CPE) of the outer porous layer and inner barrier layer, at HF and MF respectively, whilst R_{out} at HF and R_{in} at MF represent the resistance of the outer porous layer and inner barrier layer, respectively. Once the corrosion has reached the PEO/metal interface, the inner barrier layer (CPE_{in}) could be substituted by the double layer (CPE_{dl}) as well as the resistance R_{in} by the charge transfer one (R_{ct}). On the other hand, if an organic coating is used (Fig. 8 (b)), the time constant at HF can be substituted by the coating capacitance (C_c) and the resistance by the coating one (R_c). Moreover, the CPE can be translated to apparent capacitance (C_{out}, C_{in}, C_{dl} or C_c) using the equation $C_n = Y_0^{\ 1/\alpha} R_n^{(1-\alpha)/\alpha}$ [55], where R is the resistance (R_{out}, R_{in}, R_{ct} or R_c). For the sake of comparison, the apparent capacitance was also obtained for α values between 0.6 and 0.5.

Fig. 9 shows a summary of the evolution with time of the different parameters, where the resistance, apparent capacitance and α were classified as HF or MF. The idea is to differentiate between the different time constats (i.e., outer layer and epoxy coating (HF) vs. inner layer and corrosion process (MF)). Clearly, the LDH layer on the PEO-LDH system not only maintain the R value at HF with time but also it increases up to a maximum value (around 10^3 Ω·cm^2) after 28 days of immersion (Fig. 9 (a)). In contrast, the PEO system undergoes a rapid decrease larger than one order of magnitude from 1 to 7 days reaching a steady state. These findings are in agreement with smaller C_{HF} (i.e., C_{out}) at 14 and 28 days (Fig. 9 (c)), revealing that the impact of the LDH layer can be detected at HF. In fact, the best scenario occurred at 3 days with a C_{out} typical of an isolating coating (around 10^{-8} F/cm^2) and with a unique shape of the impedance diagram (Fig. 5 (d)). However, when an organic coating is used, both systems provided similar values of the C_{HF} (i.e., C_c) and a

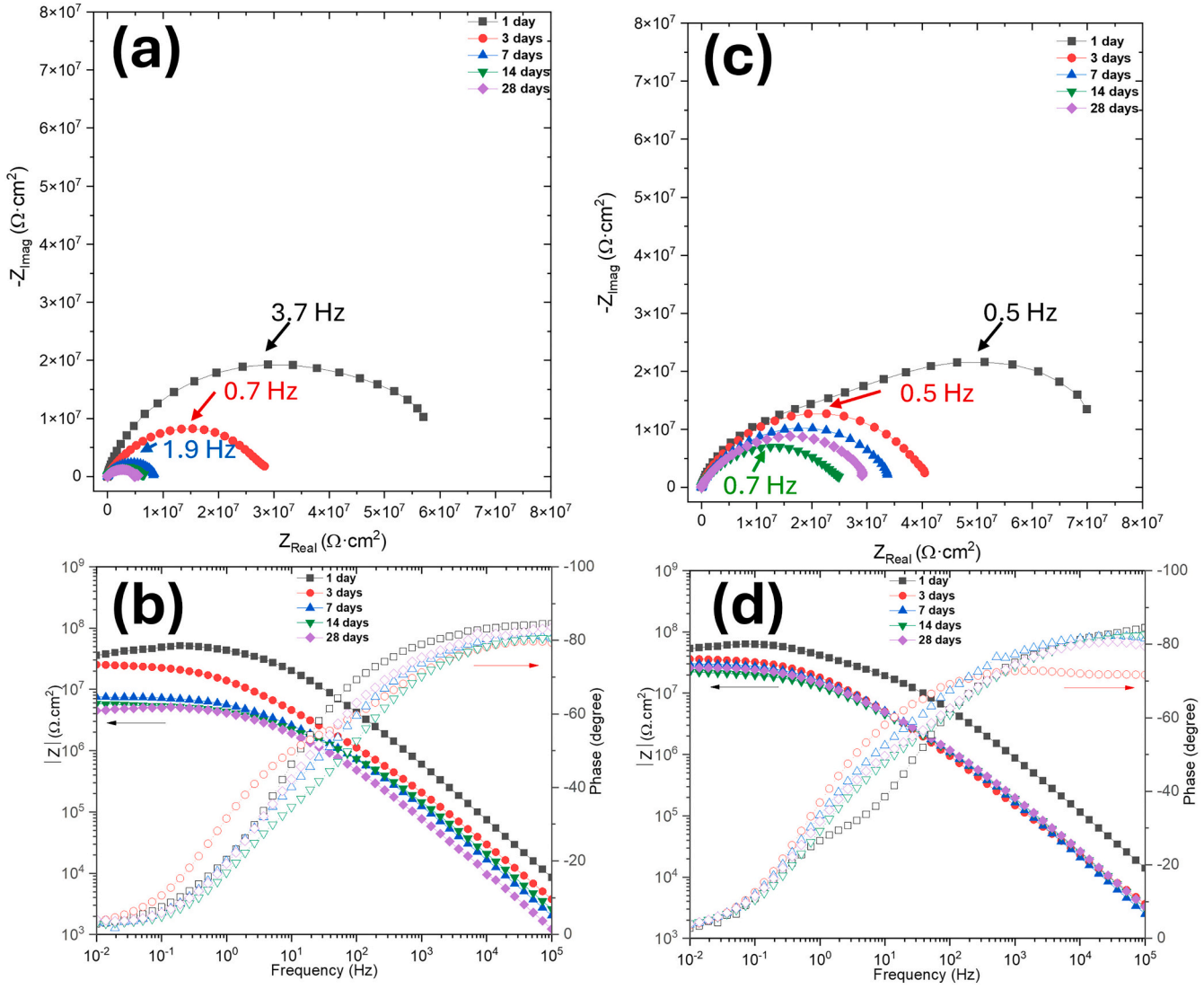

Fig. 7. Impedance diagrams (Nyquist and Bode) at different immersion time in 3.5 wt% NaCl: (a-b) PEO + Epoxy, and (c-d) PEO-LDH + Epoxy. (The Nyquist plots after 1 day of immersion do not show the last 9 and 7 points for PEO + Epoxy and PEO-LDH + Epoxy, respectively).

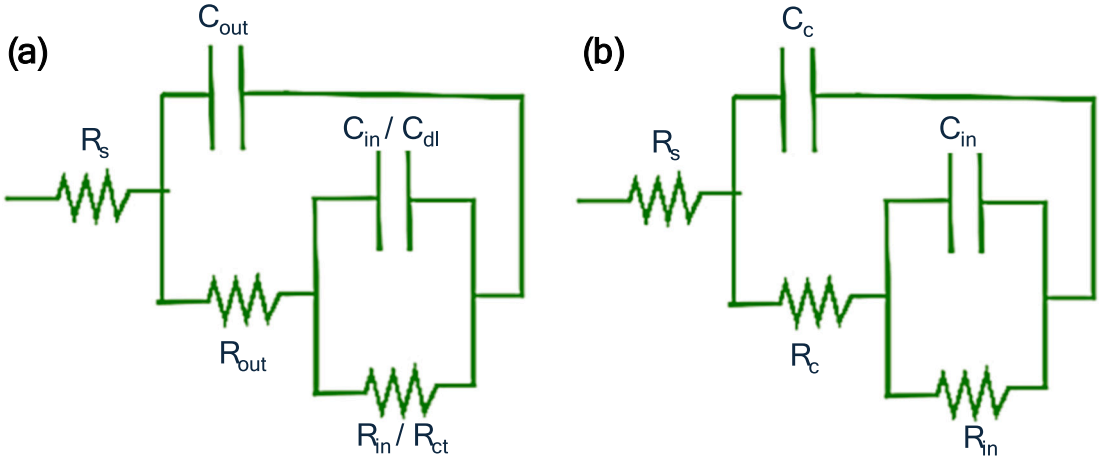

Fig. 8. Equivalent circuits used for fitting the EIS diagrams: (a) PEO and PEO-LDH, and (b) PEO + Epoxy and PEO-LDH-Epoxy.

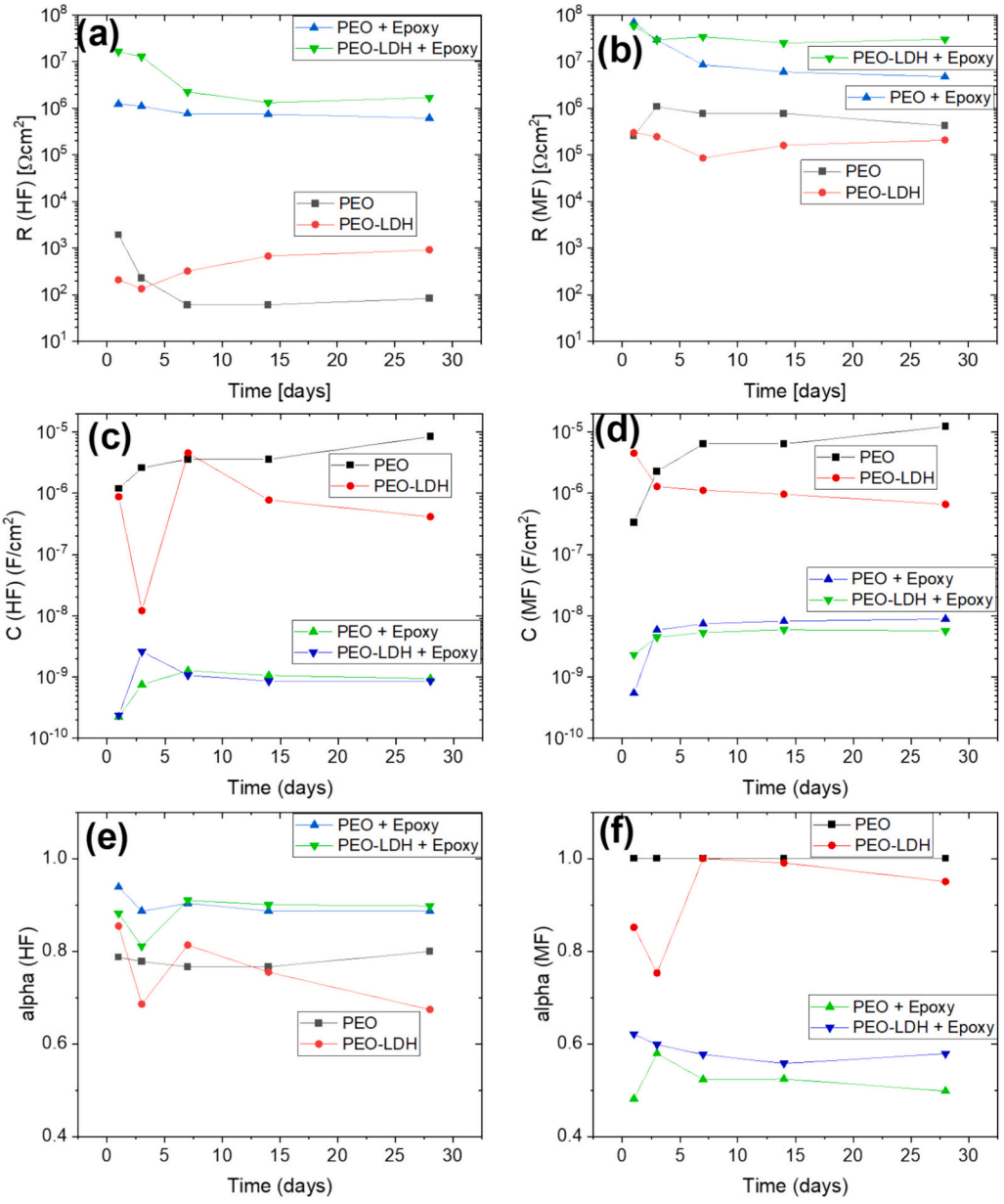

Fig. 9. Impedance parameters for PEO, PEO-LDH, PEO-Epoxy, PEO-LDH + Epoxy at different immersion times in 3.5 wt% NaCl: (a) & (b) Impedance (Z), (c) & (d) Apparent capacitance (C), and (e) & (f) "α" power of CPE obtained from the fitting.

similar trend of the R_{HF} (i.e, R_c): a smooth decrease of the impedance, although the system with LDH was showing lager values.

Regarding the MF, when an organic coating is applied, the R_{MF} (i.e., R_{in}) is larger for the PEO-LDH + Epoxy system at 7 days and such a difference reaches almost one order of magnitude at 28 days: $3.0 \cdot 10^7$ Ωcm^2 vs. $4.8 \cdot 10^6$ Ωcm^2 (Fig. 9 (b)). This finding is in agreement with the $|Z_{0.01Hz}|$ (Fig. S2 is showing a similar trend with time than the R_{in}) and confirms that the presence of LDH layer in the PEO/Epoxy interface is beneficial. In contrast, if the systems without epoxy coating are compared, the R_{MF} is slightly lower in presence of LDH. However, the most important finding can be observed in the C_{MF} values for the PEO-LDH system without epoxy (Fig. 9 (d)): not only much smaller capacitance are obtained beyond 7 days compared to PEO but also it is maintained up to 28 days ($6.6\ 10^{-7}$ F/cm^2). In fact, the PEO system shows a C_{MF} typical of a C_{dl} ($1.2\ 10^{-5}$ F/cm^2) rather than of a C_{in}. Although the C_{MF} values do not provide any additional insight with the presence of coatings, the apparent capacitance of the PEO-LDH system is still smaller than the PEO one.

Finally, (Fig. 9 (e) and (Fig. 9 (f) show the evolution with time of the α parameter at HF and MF, respectively. The most relevant aspect is shown by both systems at MF, where their α_{MF} in presence of the epoxy was below 0.6 at 3 days of immersion and beyond. Taking into account that a value around 0.5 is typical of a diffusion phenomenon, it support the not only the presence of diffusion on the PEO and PEO-LDH systems as it was stated above (Fig. 6) but also confirms that such process occurs in the interface of the PEO + Epoxy and PEO-LDH + Epoxy systems.

As a summary, the key role of the LDH seems to be in the compactness of the outer porous layer (lower CPE_{out} and higher R_{out}), in the stabilization of the barrier layer due to the lower C_{in} compared with the C_{in} of the PEO system (typical of a C_{dl}), and in the diffusion process taking place in the PEO-LDH + Epoxy system.

3.3. Adhesion

Fig. 10 shows the optical images after the adhesion tests under dry and wet conditions, with an AA2024-T3 substrate coated with epoxy

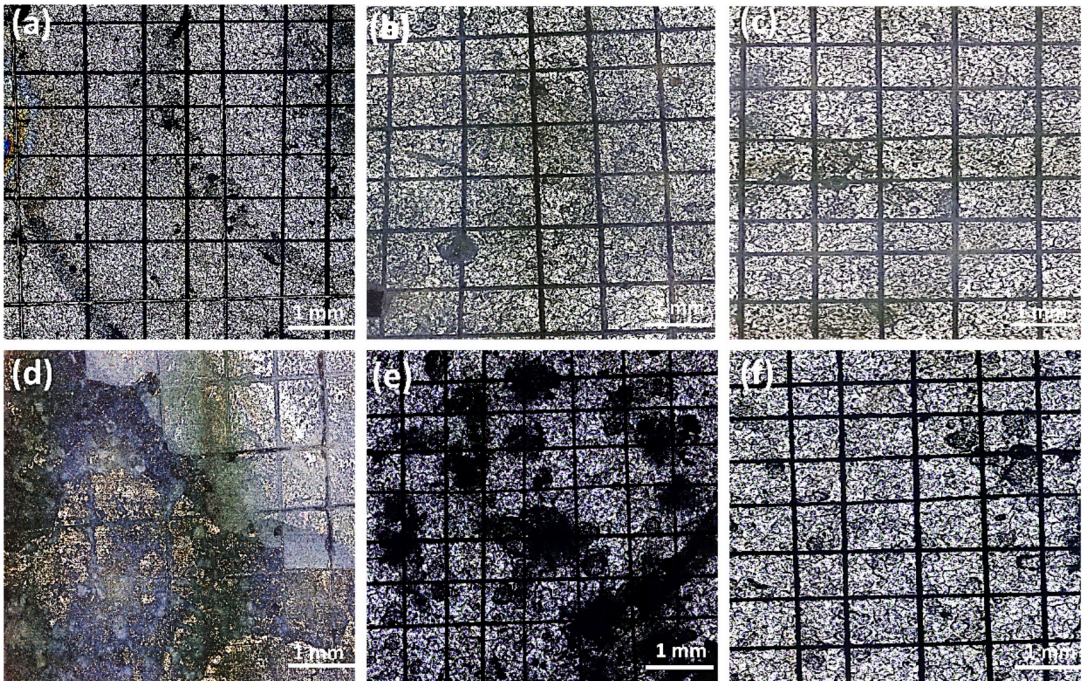

Fig. 10. Surface appearance after the adhesion test for as-prepared coatings ((a), (b) & (c)) and after 28 days of immersion in 3.5 wt% NaCl solution ((d), (e) & (f)) for: (a) & (d) Epoxy on AA2024-T3, (b) & (e) PEO + Epoxy (c) & (f) PEO-LDH-Epoxy.

serving as a reference. Under dry conditions, all systems exhibited good adhesion. However, wet adhesion results revealed notable differences: i) the reference system showed the worst performance, with the epoxy coating completely detaching. This behaviour is likely due to the high amount of corrosion products beneath the coating, ii) the PEO + Epoxy system revealed an intermediate behaviour, with the coating peeling off in several areas. Although the mechanical adhesion is favoured by the porosity and increased effective surface area of the PEO layer, the adhesion strength of this system needs to be improved, iii) the PEO-LDH + Epoxy system demonstrated the best adhesive properties, as no peeling was observed in the scratched areas. This is in agreement with the EIS results, which showed the highest impedance and lowest apparent capacitance (Fig. 9). The improved performance may be attributed to modifications in the PEO system, such as reduced porosity (Fig. 4) and lower roughness (Fig. 3), due to the LDH treatment. These modifications could enhance mechanical strength, but further analysis is necessary to understand the role of the LDH nanosheets on the surface.

3.4. Protection mechanism

The degradation of the PEO + Epoxy and PEO-LDH + Epoxy systems after prolonged immersion in a saline environment (28 days) was examined using backscattered electron SEM-EDS. The cross-sectional micrographs as well as the composition by EDS analysis of spots of interest are collected in Fig. 11 and Table 1, respectively. Immersion facilitated degradation of the protective systems, as evidenced by irregular defects and damaged zones within the epoxy layer (Fig. 11 (a & d)). Despite these defects, the metal/PEO interface appears unaffected, indicating that extensive substrate corrosion has not yet occurred. This finding discards the presence of a charge transfer reaction and double layer capacitance in the impedance diagrams for both systems.

In order to provide more insights about the degradation phenomena, Fig. 11 (b & e) presents detailed views of damaged zones from the earlier micrographs. EDS analysis of the PEO/coating interface, spot 1 (S1) for the PEO + Epoxy system, indicates the presence of oxygen (showing the largest atomic %), along with Al, Si and P from the PEO layer (indicating Al_2O_3, silicates and phosphates), and Ti and Zn from the epoxy coating (TiO_2 and Zn-based compounds). Traces of chlorides were also detected, confirming electrolyte penetration at the interface. This electrolyte intrusion appears to have compromised the integrity of the PEO/Epoxy interface, triggering delamination of the organic coating and favouring damage propagation.

In contrast, the PEO-LDH + Epoxy system exhibited a uniform PEO/Epoxy interface after immersion (Fig. 11 (e)), with minimal chloride presence at the interface (spot 1 and 2) and within the pores (spot 3 and 4). Notably, the micropores were filled with Mg, alongside Na and Mg residues from the PEO solution, confirming that Mg-Al-LDH flakes not only cover the surface (as seen in Fig. 4) but also penetrate and fill the pores of the PEO layer. This filling effect likely provides an additional barrier against electrolyte permeation (i.e., chlorides), enhancing both corrosion protection and adhesion (interlocks the PEO and the epoxy topcoat).

A similar compositional analysis conducted inside the pores of the PEO + Epoxy system (Fig. 11 (c)) reveals distinct findings. At spots 1, 2 and 3, there is no Mg detected, while the other chemical elements from the PEO layer are present. Interestingly, spot 3 also shows the presence of copper, which is associated with intermetallic particles. It is important to notice the presence of less compact Na-rich morphologies inside (and above) spot 2 that, together with the conventional pores, can facilitate the diffusion phenomena observed in the impedance diagrams of the systems without epoxy coating (Fig. 5) and corroborated by the α value at medium frequencies for both coated systems (Fig. 9 (f)).

Finally, the metal/PEO interface remains intact, as confirmed by EDS analysis at spot 1, 2 and 3 in Fig. 11 (f). These spots reveal the presence of only O, Na (in spot 3), Al and Si, which correspond to alumina and aluminium/sodium silicates. In contrast, the interface of the PEO system is already showing the presence of chlorides in such interface as it is shown in the supplementary information (Fig. S3 and Table S1). It can explain the high C_{MF} value corresponds to a C_{dl} rather than C_{in} ($1.2\ 10^{-5}$ F/cm^2, Fig. 9).

As a summary, Fig. 12 illustrate the protection mechanism with and without a LDH layer. Although the thick PEO layer provides sufficient adhesion to the epoxy coating (and no evidence of corrosion at the metal/PEO interface) after prolonged immersion in a 3.5 wt% NaCl

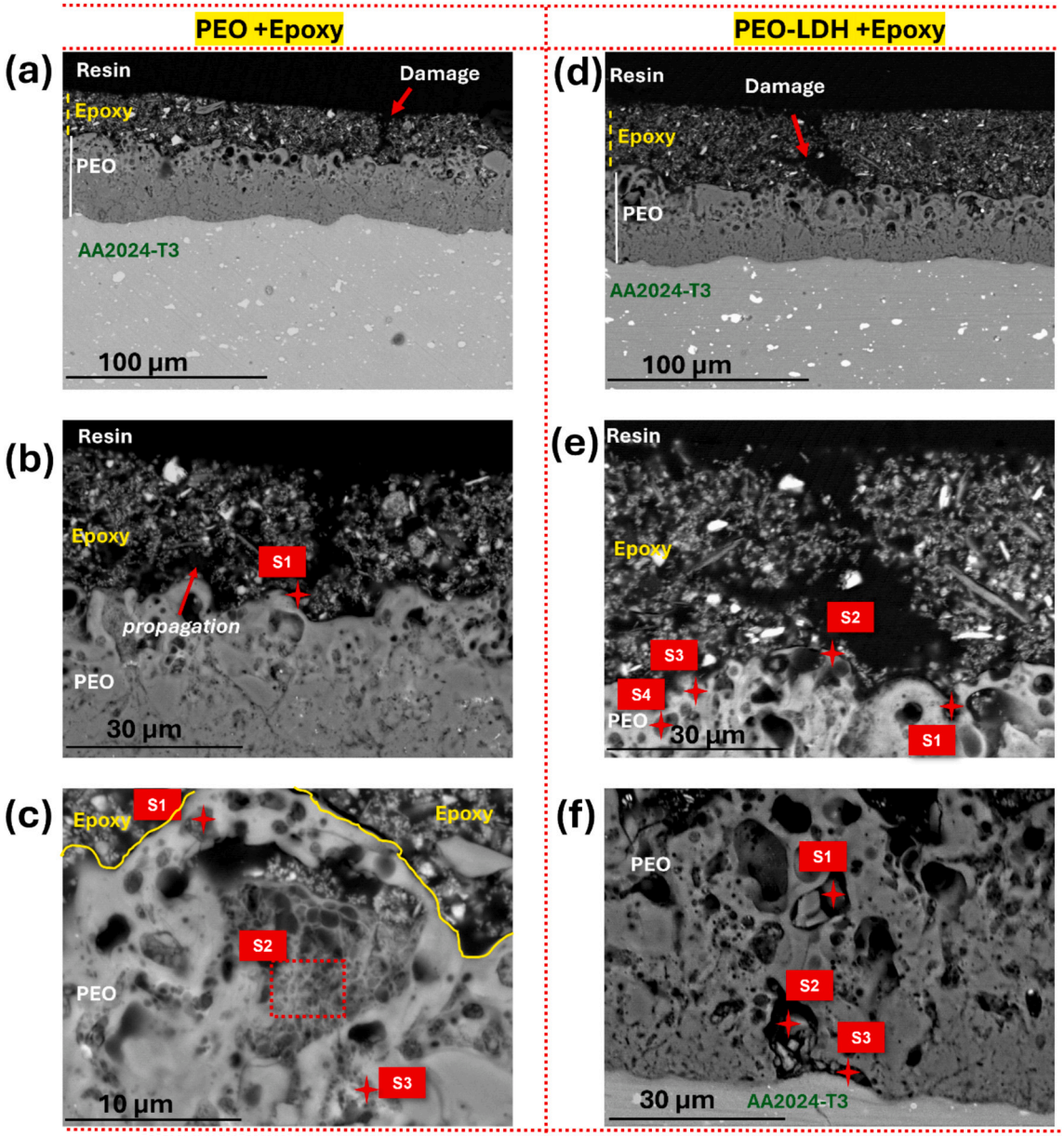

Fig. 11. Cross-sectional BS SEM images for samples immersed in 3.5 wt% NaCl for 28 days: (a), (b) & (c) PEO-Epoxy, and (d), (e) & (f) PEO-LDH + Epoxy coatings.

solution compared to the plain epoxy, the PEO/Epoxy interface shows a delamination front that undermines the adhesion between the PEO and epoxy (Fig. 12(a)). It can be explained by the penetration of water which might affect the integrity of the outer PEO layer and therefore, the bond strength of the PEO + Epoxy system. In contrast, if a LDH layer is present on the PEO surface (PEO-LDH + Epoxy system), the adhesion strength can be enhanced thanks to the following phenomena: (1) the LDH is able to penetrate into the outer layer of the PEO (filling the pores) and interlocks the PEO with topcoat epoxy, (2) the wettability of the surface might be improved with LDH during the application of the epoxy coating, strengthening the interaction LDH-epoxy (Fig. 12 (b)). Definitely, the delamination due to the penetration of the electrolyte is hindered by effective mitigation of hydration of the PEO/Epoxy interface, where the LDH is acting against the harmful effect of the electrolyte in the outer PEO layer. Indeed, the LDH layer not only covers the surface but also fills the PEO micropores, contributing to the barrier properties and mechanical integrity. It implies an improvement in the overall performance (adhesion and corrosion resistance), which is in agreement with the better EIS and wet-adhesion results compared to the PEO + Epoxy system.

4. Conclusions

MgAl-LDH films were successfully synthesized on the surface of thick, silicate-based, energy-efficient PEO layer. The surface morphology revealed a uniform network of LDH lamellae, which, according to EIS analysis, significantly delayed the intrinsic diffusion phenomena characteristic of thick, porous PEO coatings from 1 day to 14 days of immersion. The synergy of both surface treatments becomes especially evident when an epoxy coating is applied as the topmost layer. This approach notably improves wet adhesion and provides long-term corrosion protection. The LDH not only covers the surface (reducing the roughness) but also fills the pores of the PEO layer, interlocking the PEO and the organic coating. This dual action enhances the barrier properties of the system, hindering electrolyte ingress and preventing delamination of the organic coating at the PEO/epoxy interface in the PEO-LDH + Epoxy system. This approach anticipates further intercalation of corrosion inhibitors into the LDH layer, whose

Table 1
EDS results (atomic %) for the studied PEO + Epoxy and PEO-LDH + Epoxy coatings. EDS locations are labelled in.

Positions	O	Na	Mg	Al	Si	P	Cl	K	Cu	Ti	Zn
PEO + Epoxy (Fig. 11 (b))											
S1	73.8	–	–	8.9	6.7	3.6	0.5	–	–	3.9	2.6
PEO + Epoxy (Fig. 11 (c))											
S1	56.8	3.6	–	19.4	13.2	1.4	0.1	5.5	–	–	–
S2	61.6	7.2	–	12.6	14.0	0.5	–	4.1			
S3	62.7	1.5	–	17.6	13.7	0.5	–	2.2	1.8	–	–
PEO-LDH + Epoxy (Fig. 11 (e))											
S1	60.7	–	1.7	11.2	23.6	1.4	0.1	1.3	–		
S2	57.5	1.3	2.1	4.8	31.4	1.8	0.1	1.0	–		
S3	59.6	1.6	1.7	20.5	13.5	1.0	0.2	1.9	–		
S4	56.9	1.1	0.9	24.9	13.5	1.0	0.1	1.6	–		
PEO-LDH + Epoxy (Fig. 11 (f))											
S1	44.5	–	–	21.4	34.1	–	–	–	–		
S2	46.7	–	–	43.0	10.3	–	–	–	–		
S3	43.1	1.3	–	54.1	1.5	–	–	–	–		

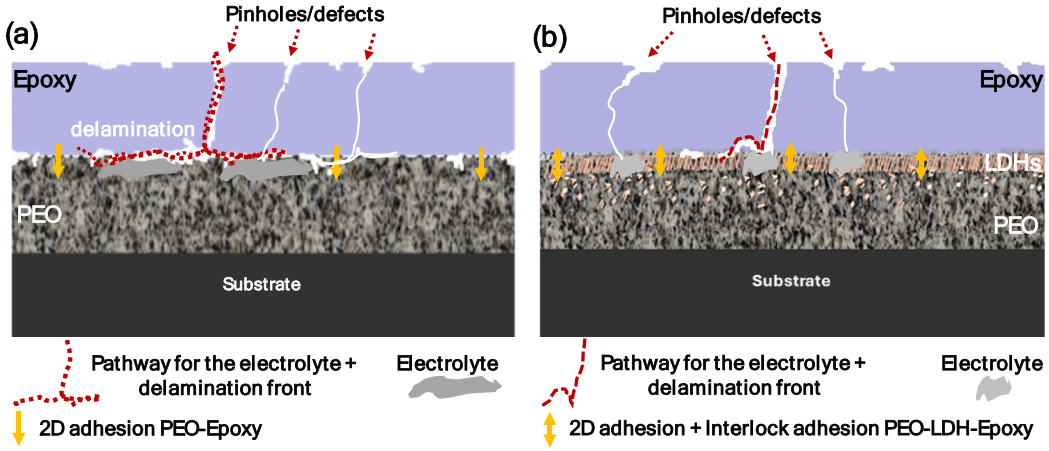

Fig. 12. Schematic illustration of the protection mechanism of the: (a) PEO-Epoxy, and (b) PEO-LDH + Epoxy systems.

direct incorporation into organic systems is often associated with adverse effects.

CRediT authorship contribution statement

Muhammad Ahsan Iqbal: Writing – original draft, Methodology, Investigation, Funding acquisition, Formal analysis, Data curation, Conceptualization. **Humaira Asghar:** Validation, Conceptualization. **Endzhe Matykina:** Writing – review & editing, Validation, Methodology. **Raúl Arrabal:** Writing – review & editing, Resources, Methodology. **Marta Mohedano:** Writing – review & editing, Supervision, Funding acquisition. **Jesús Manuel Vega:** Writing – review & editing, Validation, Methodology, Investigation, Formal analysis, Data curation, Conceptualization.

Declaration of competing interest

The authors declare that they have no known competing financial interests or personal relationships that could have appeared to influence the work reported in this paper.

Acknowledgements

This work is financed by the European project UNA4CAREER (Marie Skłodowska Curie grant No 847635). The authors also gratefully acknowledge the support of PID2021-124341OB-C22 (MCIU/AEI/FEDER, UE). J.M. Vega also acknowledges the Grant RYC2021-034384-I funded by MICIU/AEI/10.13039/501100011033 and by "European Union NextGenerationEU/PRTR".

Appendix A. Supplementary data

Supplementary data to this article can be found online at https://doi.org/10.1016/j.porgcoat.2025.109397.

Data availability

All data presented in this work will be made available through Docta Complutense repository https://docta.ucm.es/handle/20.500.14352/16

References

[1] M.Y. Jiang, L.K. Wu, J.M. Hu, J.Q. Zhang, Silane-incorporated epoxy coatings on aluminum alloy (AA2024). Part 2: mechanistic investigations, Corros. Sci. 92 (2015) 127–135, https://doi.org/10.1016/J.CORSCI.2014.11.048.
[2] J.B. Bajat, V.B. Mišković-Stanković, Z. Kačarević-Popović, Corrosion stability of epoxy coatings on aluminum pretreated by vinyltriethoxysilane, Corros. Sci. 50 (2008) 2078–2084, https://doi.org/10.1016/J.CORSCI.2008.04.018.

[3] A. Madhankumar, S. Nagarajan, N. Rajendran, T. Nishimura, EIS evaluation of protective performance and surface characterization of epoxy coating with aluminum nanoparticles after wet and dry corrosion test, J. Solid State Electrochem. 16 (2012) 2085–2093, https://doi.org/10.1007/S10008-011-1623-1/FIGURES/9.

[4] X. Chen, J. Tang, H. Wei, H. Zhang, Y. Tang, X. Zhao, Y. Zuo, Effect of cerium tartrate on the corrosion resistance of epoxy coating on aluminum alloy and its mechanism, Coatings 12 (2022) 785, https://doi.org/10.3390/COATINGS12060785.

[5] D. Zeng, Z. Liu, L. Zou, H. Wu, Corrosion resistance of epoxy coatings modified by bis-silane prepolymer on aluminum alloy, Coatings 11 (2021) 842, https://doi.org/10.3390/coatings11070842.

[6] R. Naderi, M.M. Attar, The role of zinc aluminum phosphate anticorrosive pigment in protective performance and cathodic disbondment of epoxy coating, Corros. Sci. 52 (2010) 1291–1296, https://doi.org/10.1016/J.CORSCI.2009.12.019.

[7] F. Zhang, P. Ju, M. Pan, D. Zhang, Y. Huang, G. Li, X. Li, Self-healing mechanisms in smart protective coatings: a review, Corros. Sci. 144 (2018) 74–88, https://doi.org/10.1016/J.CORSCI.2018.08.005.

[8] D. Zhang, T.K. Ronson, J.R. Nitschke, Functional capsules via subcomponent self-assembly, Acc. Chem. Res. 51 (2018) 2423–2436, https://doi.org/10.1021/ACS.ACCOUNTS.8B00303/ASSET/IMAGES/LARGE/AR-2018-00303H_0022.JPEG.

[9] P. Ctibor, K. Neufuss, F. Zahalka, B. Kolman, Plasma sprayed ceramic coatings without and with epoxy resin sealing treatment and their wear resistance, Wear 262 (2007) 1274–1280, https://doi.org/10.1016/J.WEAR.2007.01.005.

[10] S. Liscano, L. Gil, M.H. Staia, Effect of sealing treatment on the corrosion resistance of thermal-sprayed ceramic coatings, Surf. Coat. Technol. 188–189 (2004) 135–139, https://doi.org/10.1016/J.SURFCOAT.2004.08.009.

[11] Y. Bao, J. Gao, D.T. Gawne, Crack formation and its prevention in PVD films on epoxy coatings, Surf. Coat. Technol. 205 (2010) 15–21, https://doi.org/10.1016/J.SURFCOAT.2010.05.037.

[12] Y. Xu, H. Li, Y. Shen, S. Liu, W. Wang, J. Tao, Improvement of adhesion performance between aluminum alloy sheet and epoxy based on anodizing technique, Int. J. Adhes. Adhes. 70 (2016) 74–80, https://doi.org/10.1016/J.IJADHADH.2016.05.007.

[13] C. Blawert, V. Heitmann, W. Dietzel, H.M. Nykyforchyn, M.D. Klapkiv, Influence of electrolyte on corrosion properties of plasma electrolytic conversion coated magnesium alloys, Surf. Coat. Technol. 201 (2007) 8709–8714, https://doi.org/10.1016/j.surfcoat.2006.07.169.

[14] G.A. Mengesha, J.P. Chu, B.S. Lou, J.W. Lee, Corrosion performance of plasma electrolytic oxidation grown oxide coating on pure aluminum: effect of borax concentration, J. Mater. Res. Technol. 9 (2020) 8766–8779, https://doi.org/10.1016/J.JMRT.2020.06.020.

[15] L.O. Snizhko, A.L. Yerokhin, A. Pilkington, N.L. Gurevina, D.O. Misnyankin, A. Leyland, A. Matthews, Anodic processes in plasma electrolytic oxidation of aluminium in alkaline solutions, Electrochim. Acta 49 (2004) 2085–2095, https://doi.org/10.1016/j.electacta.2003.11.027.

[16] F. Simchen, M. Sieber, A. Kopp, T. Lampke, Introduction to plasma electrolytic oxidation—an overview of the process and applications, Coatings 10 (2020) 628, https://doi.org/10.3390/COATINGS10070628.

[17] X. Lu, M. Mohedano, C. Blawert, E. Matykina, R. Arrabal, K.U. Kainer, M. L. Zheludkevich, Plasma electrolytic oxidation coatings with particle additions – a review, Surf. Coat. Technol. 307 (2016) 1165–1182, https://doi.org/10.1016/J.SURFCOAT.2016.08.055.

[18] X. Lu, S.P. Sah, N. Scharnagl, M. Störmer, M. Starykevich, M. Mohedano, C. Blawert, M.L. Zheludkevich, K.U. Kainer, Degradation behavior of PEO coating on AM50 magnesium alloy produced from electrolytes with clay particle addition, Surf. Coat. Technol. 269 (2015) 155–169, https://doi.org/10.1016/j.surfcoat.2014.11.027.

[19] V. Dehnavi, B.L. Luan, D.W. Shoesmith, X.Y. Liu, S. Rohani, Effect of duty cycle and applied current frequency on plasma electrolytic oxidation (PEO) coating growth behavior, Surf. Coat. Technol. 226 (2013) 100–107, https://doi.org/10.1016/J.SURFCOAT.2013.03.041.

[20] C.B. Wei, X.B. Tian, S.Q. Yang, X.B. Wang, R.K.Y. Fu, P.K. Chu, Anode current effects in plasma electrolytic oxidation, Surf. Coat. Technol. 201 (2007) 5021–5024, https://doi.org/10.1016/J.SURFCOAT.2006.07.103.

[21] E. Matykina, R. Arrabal, P. Skeldon, G.E. Thompson, Optimisation of the plasma electrolytic oxidation process efficiency on aluminium, Surf. Interface Anal. 42 (2010) 221–226, https://doi.org/10.1002/SIA.3140.

[22] H. Li, R. Song, Z.J.-T. of N.M.S. of China, undefined. Effects of nano-additive TiO2 on performance of micro-arc oxidation coatings formed on 6063 aluminum alloy, Elsevier, 2013 (n.d.).

[23] M. Mohedano, B. Mingo, H. Mora-Sánchez, E. Matykina, R. Arrabal, Effects of pre-anodizing and phosphates on energy consumption and corrosion performance of PEO coatings on AA6082, Surf. Coat. Technol. 409 (2021), https://doi.org/10.1016/j.surfcoat.2021.126892.

[24] M. Javidi, H. Fadaee, Plasma electrolytic oxidation of 2024-T3 aluminum alloy and investigation on microstructure and wear behavior, Appl. Surf. Sci. 286 (2013) 212–219, https://doi.org/10.1016/J.APSUSC.2013.09.049.

[25] E. Matykina, R. Arrabal, A. Mohamed, P. Skeldon, G.E. Thompson, Plasma electrolytic oxidation of pre-anodized aluminium, Corros. Sci. 51 (2009) 2897–2905, https://doi.org/10.1016/j.corsci.2009.08.004.

[26] J. Yang, C. Blawert, S.V. Lamaka, D. Snihirova, X. Lu, S. Di, M.L. Zheludkevich, Corrosion protection properties of inhibitor containing hybrid PEO-epoxy coating on magnesium, Corros. Sci. 140 (2018) 99–110, https://doi.org/10.1016/J.CORSCI.2018.06.014.

[27] J.F. Nie, A.J. Morton, B.C. Muddle, D.J. Lloyd, Some aspects of the metallurgy of automotive Al alloys, 2004.

[28] M.A. Iqbal, L. Sun, A.M. LaChance, H. Ding, M. Fedel, In situ growth of a CaAl-NO 3 − −layered double hydroxide film directly on an aluminum alloy for corrosion resistance, Dalton Trans. (2020), https://doi.org/10.1039/c9dt01773a.

[29] M.A. Iqbal, M. Fedel, Effect of operating parameters on the structural growth of ZnAl layered double hydroxide on AA6082 and corresponding corrosion resistance properties, J. Coat. Technol. Res. 16 (2019) 1423–1433, https://doi.org/10.1007/s11998-019-00227-0.

[30] M.F. Montemor, D.V. Snihirova, M.G. Taryba, S.V. Lamaka, I.A. Kartsonakis, A. C. Balaskas, G.C. Kordas, J. Tedim, A. Kuznetsova, M.L. Zheludkevich, M.G. S. Ferreira, Evaluation of self-healing ability in protective coatings modified with combinations of layered double hydroxides and cerium molibdate nanocontainers filled with corrosion inhibitors, Electrochim. Acta 60 (2012) 31–40, https://doi.org/10.1016/j.electacta.2011.10.078.

[31] M.F. Muhammad Ahsan Iqbal, Protective cerium based layered double hydroxides thin films developed on anodized AA6082, Adv. Mater. Sci. Eng. 2020 (2020) 5785393, https://doi.org/10.1155/2020/5785393.

[32] G. Zhang, L. Wu, M. Serdechnova, A. Tang, C. Wang, C. Blawert, F. Pan, M. L. Zheludkevich, In-situ LDHs growth on PEO coatings on AZ31 magnesium alloy for active protection: roles of PEO composition and conversion solution, Journal of Magnesium and Alloys 11 (2023) 2376–2391, https://doi.org/10.1016/J.JMA.2021.09.001.

[33] M. Serdechnova, M. Mohedano, B. Kuznetsov, C.L. Mendis, M. Starykevich, S. Karpushenkov, J. Tedim, M.G.S. Ferreira, C. Blawert, M.L. Zheludkevich, PEO coatings with active protection based on in-situ formed LDH-nanocontainers, J. Electrochem. Soc. 164 (2017) C36–C45, https://doi.org/10.1149/2.0301702JES.

[34] T. Shulha, M. Shikun, M. Serdechnova, T. Naacke, V. Kasneryk, V. Heitmann, P. Karlova, A. Davydok, S.A. Karpushenkov, C. Blawert, M.L. Zheludkevich, Chelating agent stimulated LDH post-treatment of PEO coated AA2024, Appl. Surf. Sci. 670 (2024) 160707, https://doi.org/10.1016/J.APSUSC.2024.160707.

[35] M. Mohedano, M. Serdechnova, M. Starykevich, S. Karpushenkov, A.C. Bouali, M. G.S. Ferreira, M.L. Zheludkevich, Active protective PEO coatings on AA2024: role of voltage on in-situ LDH growth, Mater. Des. 120 (2017) 36–46, https://doi.org/10.1016/J.MATDES.2017.01.097.

[36] A.C. Bouali, E.A. Straumal, M. Serdechnova, D.C.F. Wieland, M. Starykevich, C. Blawert, J.U. Hammel, S.A. Lermontov, M.G.S. Ferreira, M.L. Zheludkevich, Layered double hydroxide based active corrosion protective sealing of plasma electrolytic oxidation/sol-gel composite coating on AA2024, Appl. Surf. Sci. 494 (2019) 829–840, https://doi.org/10.1016/J.APSUSC.2019.07.117.

[37] M. Serdechnova, M. Mohedano, B. Kuznetsov, C.L. Mendis, M. Starykevich, S. Karpushenkov, J. Tedim, M.G..S. Ferreira, C. Blawert, M.L. Zheludkevich, PEO coatings with active protection based on in-situ formed LDH-nanocontainers, J. Electrochem. Soc. 164 (2017) C36–C45, https://doi.org/10.1149/2.0301702JES/XML.

[38] G. Zhang, E. Jiang, L. Wu, A. Tang, A. Atrens, F. Pan, Active corrosion protection of phosphate loaded PEO/LDHs composite coatings: SIET study, Journal of Magnesium and Alloys 10 (2022) 1351–1357, https://doi.org/10.1016/J.JMA.2021.03.008.

[39] F. Chen, P. Yu, Y. Zhang, Healing effects of LDHs nanoplatelets on MAO ceramic layer of aluminum alloy, J. Alloys Compd. 711 (2017) 342–348, https://doi.org/10.1016/J.JALLCOM.2017.04.016.

[40] M. Serdechnova, M. Mohedano, A.C. Bouali, D. Höche, B. Kuznetsov, S. Karpushenkov, C. Blawert, M.L. Zheludkevich, Role of Phase Composition of PEO Coatings on AA2024 for In-Situ LDH Growth, Coatings 7 (2017) 190, https://doi.org/10.3390/COATINGS7110190.

[41] I. Mohammadi, T. Shahrabi, M. Mahdavian, M. Izadi, Construction of an epoxy coating with excellent protection performance on the AA 2024-T3 using ion-exchange materials loaded with eco-friendly corrosion inhibitors, Prog. Org. Coat. 166 (2022) 106786, https://doi.org/10.1016/J.PORGCOAT.2022.106786.

[42] D. Zeng, Z. Liu, S. Bai, J. Zhao, Preparation and Characterization of a Silane Sealed PEO Coating on Aluminum Alloy, Coatings 11 (2021) 549, https://doi.org/10.3390/COATINGS11050549.

[43] L. Pezzato, M. Rigon, A. Martucci, K. Brunelli, M. Dabalà, Plasma electrolytic oxidation (PEO) as pre-treatment for sol-gel coating on aluminum and magnesium alloys, Surf. Coat. Technol. 366 (2019) 114–123, https://doi.org/10.1016/J.SURFCOAT.2019.03.023.

[44] M. Mohedano, E. Lopez, B. Mingo, S. Moon, E. Matykina, R. Arrabal, Energy consumption, wear and corrosion of PEO coatings on preanodized Al alloy: the influence of current and frequency, J. Mater. Res. Technol. 21 (2022) 2061–2075, https://doi.org/10.1016/j.jmrt.2022.10.049.

[45] A. Nominé, J. Martin, G. Henrion, T. Belmonte, Effect of cathodic micro-discharges on oxide growth during plasma electrolytic oxidation (PEO), Surf. Coat. Technol. 269 (2015) 131–137, https://doi.org/10.1016/j.surfcoat.2015.01.076.

[46] M.A. Iqbal, E. Matykina, R. Arrabal, M. Mohedano, Role of anodic precursor layer thickness on PEO coatings: energy consumption and long-term corrosion performance, Surf. Coat. Technol. 476 (2024), https://doi.org/10.1016/j.surfcoat.2023.130186.

[47] E. Matykina, R. Arrabal, A. Mohamed, P. Skeldon, G.E. Thompson, Plasma electrolytic oxidation of pre-anodized aluminium, Corros. Sci. 51 (2009) 2897–2905, https://doi.org/10.1016/J.CORSCI.2009.08.004.

[48] A. Mikhailau, H. Maltanava, S.K. Poznyak, A.N. Salak, M.L. Zheludkevich, K. A. Yasakau, M.G.S. Ferreira, One-step synthesis and growth mechanism of nitrate intercalated ZnAl LDH conversion coatings on zinc, Chem. Commun. 55 (2019) 6878–6881, https://doi.org/10.1039/C9CC02571E.

[49] S. Shang, A. Hanif, M. Sun, Y. Tian, Y. Ok, K.I.-J. of hazardous, undefined. Novel M (Mg/Ni/Cu)-Al-CO3 layered double hydroxides synthesized by aqueous miscible organic solvent treatment (AMOST) method for CO2 capture, ElsevierS Shang, A Hanif, M Sun, Y Tian, YS Ok, KM Iris, DCW Tsang, Q Gu, J ShangJournal of Hazardous Materials, 2019•Elsevier (n.d.), 2019, https://www.sciencedirect.com/science/article/pii/S0304389419303590?casa_token=ZJbXNYLheLAAAAAA:fMuz2Ri4A6qQapK2UF19k9qZl4_rZ8qVkZGkmr5OimCof1rrKqPFjLLOeGz1BQ67XCGQwENlEAA (accessed November 30, 2024).

[50] E. Matykina, R. Arrabal, P. Skeldon, G.E. Thompson, Investigation of the growth processes of coatings formed by AC plasma electrolytic oxidation of aluminium, Electrochim. Acta 54 (2009) 6767–6778, https://doi.org/10.1016/j.electacta.2009.06.088.

[51] A.L. Yerokhin, X. Nie, A. Leyland, A. Matthews, S.J. Dowey, Plasma electrolysis for surface engineering, Surf. Coat. Technol. 122 (1999) 73–93, https://doi.org/10.1016/S0257-8972(99)00441-7.

[52] A. Mikhailau, H. Maltanava, S.K. Poznyak, A.N. Salak, M.L. Zheludkevich, K. A. Yasakau, M.G.S. Ferreira, One-step synthesis and growth mechanism of nitrate intercalated ZnAl LDH conversion coatings on zinc, Chem. Commun. 55 (2019) 6878–6881, https://doi.org/10.1039/C9CC02571E.

[53] M.A. Iqbal, L. Sun, A.T. Barrett, M. Fedel, Layered Double Hydroxide Protective Films Developed on Aluminum and Aluminum Alloys: Synthetic Methods and Anti-Corrosion Mechanisms, Coatings 10 (2020) 428, https://doi.org/10.3390/COATINGS10040428.

[54] S. Feliu, J.M. Bastidas, J.C. Galvan, J. Simancas, M. Morcillo, E. Almeida, Electrochemical determination of rusted steel surface stability, J. Appl. Electrochem. 23 (1993) 157–161, https://doi.org/10.1007/BF00246953/METRICS.

[55] C. Hsu, F. Mansfeld, Concerning the conversion of the constant phase element parameter Y0 into a capacitance, Corrosion 57 (2001), https://doi.org/10.5006/1.3280607.

[56] Y. Ben Amor, E.M.M. Sutter, H. Takenouti, M.E. Orazem, B. Tribollet, Interpretation of electrochemical impedance for corrosion of a coated silver film in terms of a pore-in-pore model, J. Electrochem. Soc. 161 (2014) C573–C579, https://doi.org/10.1149/2.1151412JES/XML.